A novel modelling framework for immunity-driven epidemics of non-sterilising infections

Daniel Stocks (Daniel.Stocks@bristol.ac.uk)[1], Amy C Thomas (AmyC.Thomas@bristol.ac.uk)[2], Ellen Brooks-Pollock (Ellen.Brooks-Pollock@bristol.ac.uk)[2,3], and Leon Danon (L.Danon@bristol.ac.uk)[1,3]

[1]Department of Engineering Mathematics, University of Bristol
[2]Population Health Sciences, Bristol Medical School, University of Bristol
[3]Equal contribution

Abstract

Protecting populations against infections with non-sterilising immunity, such as COVID-19 and influenza, presents a major public health challenge. Unlike other infections, COVID-19 has produced irregular epidemic dynamics that are not fully explained by seasonal behavioural patterns. New variants and waning immunity require repeated vaccination, but the population models used to guide these strategies are often incompatible with individual-level immunological and virological data. To address this gap, we develop a novel and flexible mathematical framework that links within-host immune and viral dynamics to between-host transmission, bridging multiple scales from individuals to populations.

Our approach combines a mechanistic description of viral load and antibody responses, fit to qPCR data from a COVID-19 human challenge study, with population-level transmission dynamics. Specifically, we link infectiousness to viral load and protection against reinfection to time-varying level of immune factors, allowing population-level epidemiological trajectories to emerge as the summation of individual infectiousness and immunity. Using previously parameterised models of COVID-19 antibody dynamics and a mechanistic model of viral load, we compare this framework to conventional compartmental models and demonstrate its ability to predict times to reinfection and the number of infections experienced by individuals.

We show that the immune profile within individuals fundamentally shapes epidemic dynamics. Successive epidemic waves consist of overlapping immune histories, with their characteristics determined by the degree of cross-protection between infections and vaccination. Low correlations between antibody levels and protection lead to frequent reinfections and

endemic circulation, whereas high correlations produce recurrent, explosive outbreaks. Model parameters can be recovered by fitting to simulated case data, indicating that the framework can be adapted to real-world surveillance data to estimate the protective power and dynamics of diverse immune histories. This transdisciplinary approach provides new insights into the drivers of irregular epidemic patterns and can inform vaccination strategies for pathogens with non-sterilising immunity.

1 Introduction

Vaccination and infection can prevent (re)infection and the development of clinical disease by inducing an immune response within individuals. Immune responses constitute a complex web of often simultaneous interactions between stimuli, immune cells, and effector proteins that are stimulated to proliferate and subsequently wane at different times and rates post-exposure (1). These individual-level within-host processes and resulting protective mechanisms play a key role in driving population-level epidemiological dynamics (2). Understanding how immunity to a disease changes over time is vital for accurately predicting future epidemic trajectories and optimising vaccine strategies (3; 4).

For diseases such as COVID-19, mumps, and malaria, for which immunity is non-sterilising and wanes over time (5; 6; 7), reinfection and repeat outbreaks (8; 9) are commonly observed. The relationship between immune dynamics and protection from infection is commonly described in terms of correlates and surrogates of protection. A correlate of protection is an immune function that is responsible for protection (10). A surrogate of protection is an easier to measure immune function that is correlated with an immune function responsible for protection that may be unknown or difficult to measure. Typically, surrogates and correlates of protection are defined as the level required to achieve a desired probability of protection against infection (or severe disease) (11). However, a continuous relationship between the surrogate/correlate level and the probability of protection is more informative. This profile of protection would enable understanding of how within-host dynamics manifest as waning immunity and subsequently drive epidemics.

The wealth of data collected during the COVID-19 pandemic offers a unique opportunity to reflexively develop methodologies that estimates profiles of protection. Inoculating rhesus macaques with Spike protein-expressing adenovirus and DNA vaccines against SARS-CoV-2 has shown that neutralising antibody (nAb) titres negatively correlate with viral load at the peak, and at 14 and 28 days post-exposure (12; 13). Mean nAb titers in people have also been correlated with reported vaccine efficacy against infection (14), and a non-linear relationship between mean nAb titers and vaccine efficacy against infection has been established (15). These studies, amongst others (16), demonstrate that nAb titers are associated with protection in people, but do not account for waning antibody levels inhibiting assessments of how immunity changes over time.

A more general relationship between antibody level and the probability of receiving a positive polymerase-chain reaction (PCR) test result has been estimated by fitting a general additive logistic model at different antibody concentrations 21 - 59 days prior to the test (17). Combining these results with temporal profiles of antibody levels post-vaccination begins to help us understand how protection against infection varies over time. However, this observational methodology does not account for varying infection pressure. These data were collected between the 8th of December 2020 and the 4th October 2021. Although most of the cases in the interval were of the same variant (delta) (18), prevalence levels, driven by behavioural factors including non-pharmaceutical social interventions, varied substantially (19). Hence, individuals vaccinated at different times during the epidemic will experience different infection pressures and therefore have different likelihoods of being infected even if they have the same level of antibody. To disentangle the effects of infection pressure and individual protection, individual immunity post-exposure can be incorporated as part of population-level mathematical model of disease dynamics.

The most widely used mathematical models are compartmental, which categorise individuals into stages of infection and assume a constant rate of transition between categories, resulting in exponentially distributed recovery times and duration of immunity (20). These simplifying assumptions do not capture the complexity of within-host dynamics. More realistic waiting-time distributions, such as normal and gamma distributions, can be approximated in compartmental models by expanding the number of compartments in the infectious and recovered classes, creating discretised versions of integrodifferential equations (21; 22; 23). In accounting for time since infection, such expansions to compartmental models allow for varying infectiousness and protection (24; 3; 25) or varying rates of recovery and waning immunity (23; 26; 27) post exposure, which, if informed by within-host models, can link within-host and epidemiological dynamics.

The challenge of linking within-host and epidemiological dynamics with integrodifferential compartmental models is validating assumptions about the impact of within-host dynamics on immunity and infectivity. Estimated profiles of protection can be validated by comparing the timing of (re)infection predicted by a model to those recorded empirically. Infection times can be estimated from longitudinal serological measurements (28) as well as classification of PCR positive and negative samples. However, for compartmental models to track reinfection, an entirely separate system of equations is needed for each potential reinfection, which becomes computationally expensive with high numbers of reinfections and requires prior assumptions about reinfection dynamics. Consequently, models usually only track a single reinfection, if any, and rarely estimate the rate of reinfection (29; 30; 31).

We propose a novel modelling framework that tracks all reinfections and accounts for variation in immunity and infectivity based on time since infection. The framework can be informed by within-host dynamics, enabling the estimation and validation of profiles of protection. As an example, we use previously observed antibody levels following COVID-19 vaccination (32) and fit

Infectivity-Immunity Convolution Model		
Parameter	Description	Units
ξ	average contact rate	days^{-1}
$P_I(h)$	probability of being infectious h time post-infection	–
$P_S(h)$	probability of being susceptible to infection h time post-infection	–
Compartmental Models		
ξ	average contact rate	days^{-1}
η	probability of being infectious	–
δ	probability of being immune	–
$\frac{1}{\phi}$	average time until recovery	days
$\frac{1}{\lambda}$	average time until constant immunity	days
Antibody Model (32)		
A_0	initial antibody level	Ab
Φ_s	plasmablast antibody production capacity	cells $\cdot$ Ab $\cdot$ days^{-1}
Φ_l	plasmacell antibody production capacity	cells $\cdot$ Ab $\cdot$ days^{-1}
μ_s	average plasamblast decay rate	days^{-1}
μ_a	average antibody decay rate	days^{-1}
Viral Load Model		
d	horizontal shift	–
α	rate parameter	–
κ	scale parameter	–

Table 1: The description and units of parameters and functions used in respective models. Ab is an abbreviation of antibodies.

a phenomenological model to longitudinal quantitative PCR (qPCR) data collected from the throats of 18 previously naive 18 to 29 year-olds challenged with wild-type SARS-CoV-2 (33). We demonstrate how within-host models can be transformed into probabilities of being susceptible and infectious at any given time post-infection, and subsequently simulate epidemic dynamics. We demonstrate how the parameters used to simulate an epidemic can be recovered when the model is fit to daily and weekly testing data, and therefore how profiles of protection can be estimated from population-level data and validated by serological observations.

2 The Infectivity-Immunity Convolution Model

Instead of categorising people by their stage of infection (e.g. susceptible, infectious, recovered) as compartmental models do, we categorise them by when they were last infected. This way, everyone last infected the same amount of time ago will have the same infectiousness and susceptibility to infection. Hence, people will be both partially protected and partially infectious simultaneously. The level of infectiousness, $I_n(t)$, and susceptibility, $S(t)$, in the population as a function of time, t, are modelled, rather than the proportion of people in each

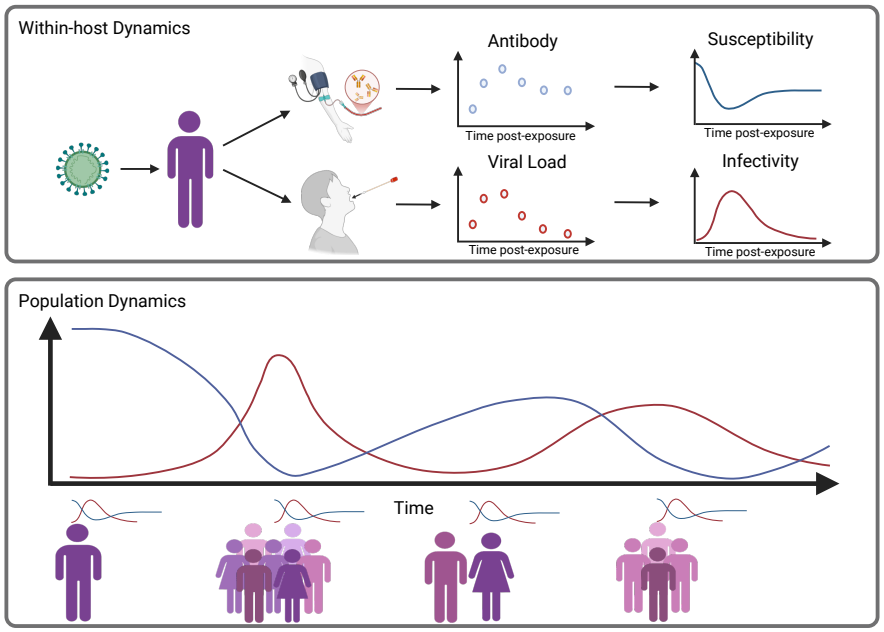

Figure 1: The within-host dynamics are summarised as susceptibility and infectivity. These quantities are estimated from immune factor data (such as antibodies) and viral load post-exposure. The population dynamics are the cumulative susceptibility and infectivity of individuals who have been exposed.

stage of infection.

Defining $P_I(h)$ and $P_S(h)$ as the average probability of being infectious and susceptible, respectively, h time after last being infected, the infectivity immunity convolution (IIC) model is:

$$S(t) = S_0\,\theta_t^{S_0} + I_0^I \theta_{0,t}^S\,P_S(t) + \xi \int_0^t S(\tau)\,I_n(\tau)\,\theta_{\tau,t}^S\,P_S(t-\tau)\,d\tau, \tag{1a}$$

$$I_n(t) = I_0\,\theta_{0,t}^S\,P_I(t) + \xi \int_0^t S(\tau)\,I_n(\tau)\,\theta_{\tau,t}^S\,P_I(t-\tau)\,d\tau, \tag{1b}$$

$$\theta_t^{S_0} = \exp\left(-\xi \int_0^t I_n(h)\,dh\right), \tag{1c}$$

$$\theta_{\tau,t}^S = \exp\left(-\xi \int_0^{t-\tau} P_S(h)\,I_n(\tau+h)\,dh\right), \tag{1d}$$

where ξ is the average contact rate, $\theta_t^{S_0}$ is the probability of having a primary infection at time t, and $\theta_{\tau,t}^S$ is the probability a person is reinfected at time t given they were last infected a time τ. The probability of reinfection at each time is dictated by the infectious pressure experienced, $\xi I_n(\tau + s)$, and the probability of being susceptible while experiencing that pressure; 1 if not yet infected, and $P_S(h)$ when a person's last infection occurred h units time ago.

2.1 Numerical solutions of the IIC model

Equations (1) are coupled Volterra integrals with nonlinear kernels dependent on the variables being solved for. They cannot be solved analytically, and there are no standard packages for solving them numerically. However, when equations (1) are approximated by the trapezium rule, the equations for $I(t)$ and $S(t)$ become simultaneous equations and can be rearranged to depend only on previous values of I and P (see Appendix A). IN this way, equations (1) can be solved iteratively.

3 Comparative Compartmental Model

Conventional models of disease spread are compartmental, such as the SIR model and the SIRS model with alteration such as partial immunity in the recovered class. We refer to models with partial immunity as SIRpi models. These models, in their simplest form, assume a person's immune response and viral load behave identically at all times post-infection, only changing the moment they recover and then remaining constant again. To incorporate evolving immune responses and infectious dynamics the number of compartments in the I and R classes can be increased (34; 35; 36). Here we use n infectious states with different levels of infectiousness, η_i, and m recovered states with different levels of immunity, δ_j. In an SIRpi framework, the mth recovered state will not be transitioned out of unless a person is reinfected. We denote the average time

until recovery as $\frac{1}{\phi}$, and the average time to reach the final recovered state as $\frac{1}{\lambda}$. The SIRpi model with multiple states is then,

$$\dot{S}(t) = -\xi S(t) \sum_{i=1}^{n} \eta_i I_i(t), \tag{2a}$$

$$\dot{I}_1(t) = \xi \sum_{i=1}^{n} \eta_i I_i(t) \Big(S(t) + \sum_{j=1}^{m} \delta_j R_j(t) \Big) - n\phi I_1, \tag{2b}$$

$$\dot{I}_i(t) = n\phi(I_{i-1}(t) - I_i(t)), \tag{2c}$$

$$\dot{R}_1(t) = n\phi I_n(t) - (m-1)\lambda R_1(t) - \xi\delta_1 R_1(t) \sum_{i=1}^{n} \eta_i I_i(t), \tag{2d}$$

$$\dot{R}_j(t) = (m-1)\lambda(R_{j-1}(t) - R_j(t)) - \xi\delta_j R_j(t) \sum_{i=1}^{n} \eta_i I_i(t), \tag{2e}$$

$$\dot{R}_m(t) = (m-1)\lambda R_{m-1}(t) - \xi\delta_m R_m(t) \sum_{i=1}^{n} \eta_i I_i(t). \tag{2f}$$

In this model, newly infected individuals enter I_1. Infected individuals then move from the ith infectious state to the $(i+1)^{th}$ infectious state at a rate $n\phi$ until they are in the nth infectious state and transition into the first recovered state, R_1. Recovered individuals transition from the jth recovered state to the $(j+1)^{th}$ recovered state at a rate $(m-1)\lambda$ until they are in the mth recovered state. They remain in the mth recovered state, with the same level of partial immunity (referred to as constant immunity from here), until they are reinfected. An individual's probability of being infectious in state I_i is η_i and susceptible in state R_j is δ_j.

An SIRS formulation of this model would have individuals in the mth recovered state transition back to the susceptible state. The SIRpi formulation is used to keep the assumptions about immunity comparable with those of the IIC model.

4 Tracking Reinfection

In the compartmental model, it is not possible to track how many times a person has been infected unless a set of states is defined for each new infection. This greatly increases the computational cost of the model, and the number of times a person can be reinfected must be known/assumed beforehand.

However, in the IIC model reinfections are organically tracked through $\theta^S_{\tau,t}$. The probability of reinfection at time t for individuals infected at time τ is given by the adjoining probability density function of the survival function $\theta^S_{\tau,t}$. Hence, the transition matrix for reinfection is given by,

$$\mathbf{\Theta}_S = \frac{d}{dt}(1 - \theta^S_{\tau,t}) = \xi P_s(t-\tau) I_n(t) \theta^S_{\tau,t}, \tag{3}$$

a $T \times T$ matrix, where T is the maximum time. All elements of the lower triangle are zero, as a person cannot be reinfected before they are infected.

Since reinfection in the IIC is a Markovian process, raising $\mathbf{\Theta}_S$ to the power of r gives the probability of being infected at time τ and then reinfected for the rth time at time t.

The transition matrix $\mathbf{\Theta}_S$ is only for reinfections. The probability of being initially infected at time t is given by,

$$\mathbf{\Theta}_{S_0} = \frac{d}{dt}(1 - \theta^{S_0}_{\tau,t}) = \xi I_n(t)\theta^{S_0}_{\tau,t}, \tag{4}$$

a $1 \times T$ vector.

5 Within-host dynamics

The parameters ϕ, λ, η, and δ, and the functions $P_I(h)$ and $P_S(h)$ define the magnitude and longevity of infectiousness and protection, so realistic values and forms of them are important for accurately predicting cases. It is possible to inform these parameters and functions with virological and immunological data, such as viral load (obtained by qPCR) and level of antibody (binding and/or neutralising), if we assume they are proxies for infectiousness and immunity with higher levels indicating a greater infectiousness and immunity.

Viral load at time h following infection at $h = 0$ can be represented by the function (see Appendix B)

$$V(h) = (h + d)^{\alpha-1} e^{-\kappa(h+d)}, \tag{5}$$

where d shifts the function to allow for non-zero values at $h = 0$ and α and κ are shape and rate parameters. A mechanistic description of antibody levels at time h following infection at $h = 0$ is (32)

$$A(h) = \frac{\Phi_l}{\mu_a} + \frac{\Phi_s}{\mu_a - \mu_s} e^{-\mu_s h} + \left(A_0 - \frac{\Phi_l}{\mu_a} - \frac{\Phi_s}{\mu_a - \mu_s} \right) e^{-\mu_a h}, \tag{6}$$

where μ_a and μ_s are the decay rates of antibodies and short-lived plasma cells respectively, Φ_s and Φ_l are the productive capacities of short-lived and long-lived plasma cells respectively, and A_0 is the initial level of antibody.

5.1 Estimating rate of recovery and immune waning in the compartmental model

Given a threshold for viral load, T_V, over which a person is considered infectious, and a value just above the asymptote for antibody, T_A, we can estimate the mean time of infection, $\frac{1}{\phi}$, and the mean time until constant immunity, $\frac{1}{\lambda}$, by setting equation (5) to T_V and equation (6) to T_A. Setting T_V to the lower limit of quantification of a qPCR test, 10^3 (33), $\frac{1}{\phi}$ is estimated as lognormally distributed with a mean of 15.5 days and log standard deviation of 0.0189 days. Setting T_A to 10% above $\frac{\Phi_l}{\mu_A}$, $\frac{1}{\lambda}$ is estimated to be lognormally distributed with a mean of 228 days and log standard deviation of 0.287.

5.2 Forms of $P_I(h)$ and $P_S(h)$

In the ICC model $P_I(h)$ and $P_S(h)$ represent whole profiles of infectiousness and immunity post-infection. Given functions $A(h) : \mathbb{R}^+ \mapsto \mathbb{R}^+$ and $V(h) : \mathbb{R}^+ \mapsto \mathbb{R}^+$ of any form, that describe antibody and viral load respectively from the start of an infection ($h = 0$), we can constrain $A(h)$ and $V(h)$ between 0 and 1 using a logistic function,

$$G(x; K) = \frac{x}{x + K}, \tag{7}$$

translating viral load and antibody level into the probabilities of being infectious and susceptible to infection.

We then build infectious and susceptibility profiles as

$$P_I(h) = G(V(h); K_V), \tag{8}$$

$$P_S(h) = \begin{cases} 0 & h \leq \frac{1}{\phi}, \\ 1 - G(A(h); K_A) & h > \frac{1}{\phi} \end{cases} \tag{9}$$

We define $P_S(h)$ as 0 for $h \leq \frac{1}{\lambda}$ so that it aligns with the assumptions of compartmental models (for comparative purposes) and to account for faster-acting immune processes (such as the innate immune system) that will also contribute to an individual's immunity.

Figure 2 shows $P_I(h)$ and $P_S(h)$ when $K_V = 3\times10^6$ and $K_A = 2\times10^3$ (values chosen to give an R_0 similar to that of a coronavirus) and the parameters fit in Appendix B are used in equation (5) and the parameters for the 16 – 34 year-olds from (32) were used in equation (6). The infectious profile tends to zero

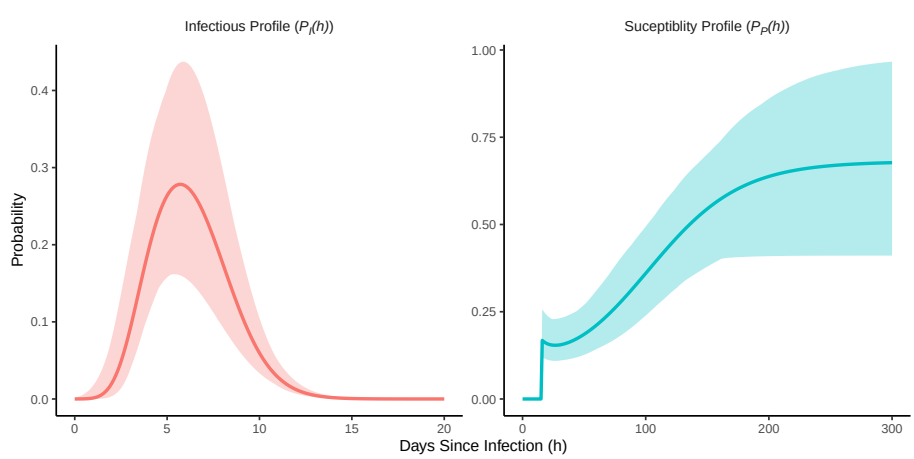

Figure 2: The infectious and susceptibility profiles post-infection. The solid line is the best fit and the shaded regions are the 95% CrI of the profiles. In these plots $K_V = 3 \times 10^6$ and $K_A = 2 \times 10^3$.

as time time tends to infinity. The susceptibility profile tends to $1 - \frac{\Phi_l}{\Phi_l + \mu_a K_A}$ which is only one when $\Phi_l = 0$.

5.3 Estimating probability of being infectious and susceptible in the compartmental model from $P_I(h)$ and $P_S(h)$

Given that η is the probability of being infectious and δ is the probability of being protected, they can be calculated as the average values of the infectious and protective profiles, over the course of the infection,

$$\eta = \phi \int_0^{\frac{1}{\phi}} P_I(h)\, dh, \tag{10}$$

$$\delta = \lambda \int_{\frac{1}{\phi}}^{\frac{1}{\phi}+\frac{1}{\lambda}} P_S(h)\, dh. \tag{11}$$

Hence, η is estimated to be lognormally distributed with mean 0.0937 and log standard deviations 0.160 day^{-1}, and δ log-normally distributed with mean 0.219 day^{-1} and log standard deviation 9.70 $\times 10^{-2}$ day^{-1}.

When there are multiple infectious and recovered compartments, the average values of the infectious and protective profiles within the intervals can be used to estimate η_i and δ_j,

$$\eta_i = n\phi \int_{\frac{i-1}{n\phi}}^{\frac{i}{n\phi}} P_I(h)\, dh, \tag{12}$$

$$\delta_j = \begin{cases} (m-1)\lambda \int_{\frac{1}{\phi}+\frac{j-1}{(m-1)\lambda}}^{\frac{1}{\phi}+\frac{j}{(m-1)\lambda}} P_S(h)\, dh, & j < m \\ P_S(\infty). & j = m \end{cases} \tag{13}$$

The definition of δ_j is piecewise because in compartments R_j for $j < m$ an individual is transitioning towards constant immunity. $P_P(\infty)$ is the asymptote of the protective profile.

6 The dynamics of the IIC and SIR-type models

Using the best fitting parameter for equations (5) and (6), the resulting infectious period, $\frac{1}{\phi}$, and $\frac{1}{\lambda}$, which is the immune period in the SIRS model but the time until constant immunity in the multicompartment SIRpi model (table 2), as well as the resulting values of η and δ (see figure 3) we can simulate an epidemic and compare the dynamics of the models. As ϕ and λ are used to calculate η and δ related ϕ-η and λ-δ pairs are used to simulate the epidemic.

Figure 4 shows the infectivity and susceptibility curves produced by each of the models. The SIR model predicts a single small wave followed by a fully immune population. The SIRS model predicts multiple small and slow waves.

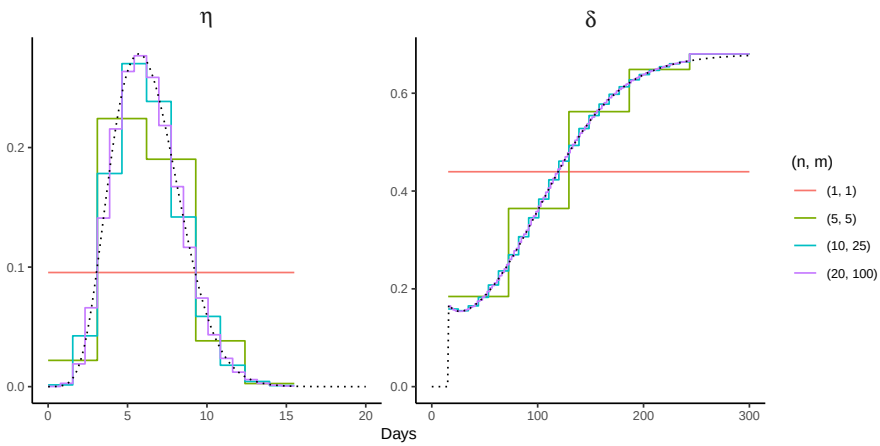

Figure 3: The probability of being infectious, η, and susceptible, δ, post-infection/recovery when different numbers of infectious and recovered compartments are used, (n, m). The dotted line is $P_I(h)$ in the graph of η is and $P_S(h)$ in the graph of δ.

When there is only one I and one R compartment in the SIRpi model it predicts a single wave followed by a constant endemic disease. As the number of compartments increases, so does the size of the waves. However, even when there are 20 infectious compartments and 100 recovered compartments the model still predicts a smaller epidemic than the IIC model. This suggests that compartmental models underestimate waves when infectivity and immunity vary post-infection. The predicted epidemics in figure 4 also suggest that assuming complete immunity post-infection (the SIR model), even if it is temporary (the SIRS model), can lead to future waves being mistimed, underestimated, or missed entirely if

Viral Load Model				
d		α		κ
1.53		15.2		1.96
Antibody Model				
μ_A	μ_S	Φ_S	Φ_l	A_0
0.0264	0.0548	1140	24.8	29.0
Days in I and R				
$\frac{1}{\phi}$			$\frac{1}{\lambda}$	
15.5			228	

Table 2: The best fitting parameter estimates for the models of viral load and antibody, and the estimates for days in I and R compartments (for the multi-compartmental SIRpi model $\frac{1}{\lambda}$ is the time until constant immunity).

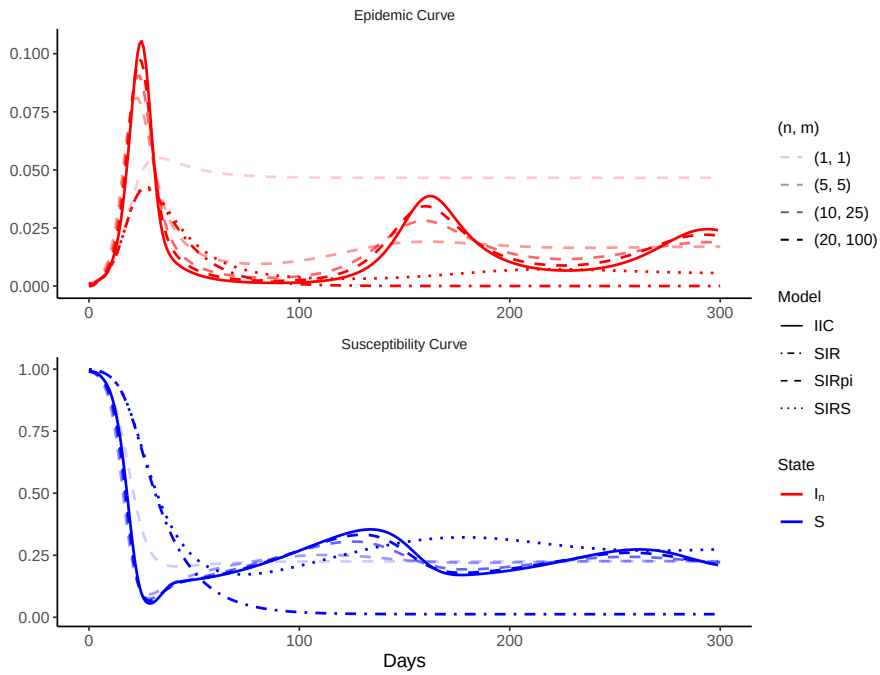

Figure 4: The infectivity and susceptibility curves of the SIR, SIRS, SIRpi, and IIC models. The infectivity curve is the total infectiousness in the population, I_n. For the compartmental models $I_n(t) = \sum_{i=1}^{n} \eta_i I_i(t)$. In the IIC model, I_n is an existing state. The susceptibility curve is the total susceptibility, either through waning immunity or lack of infection. For the compartmental models $S = S(t) + \sum_{j=1}^{m} \delta_j R_j(t)$. In the ICC model, S is an existing state.

immunity is not actually complete.

7 Reinfections in the ICC model

The oscillating dynamics in figure 4 suggest there is reinfection. By examining the transition matrix, Θ_S, and decomposing the incidence we can understand exactly what the reinfection dynamics are. Figure 5 shows the transposed transition matrices for 2nd, 3rd, and 4th infections ($\mathbf{\Theta}_S$, $\mathbf{\Theta}_S^2$, $\mathbf{\Theta}_S^3$, respectively) with each row weighted by the incidence at that time, as well as the proportion of daily incidence resulting from each reinfection.

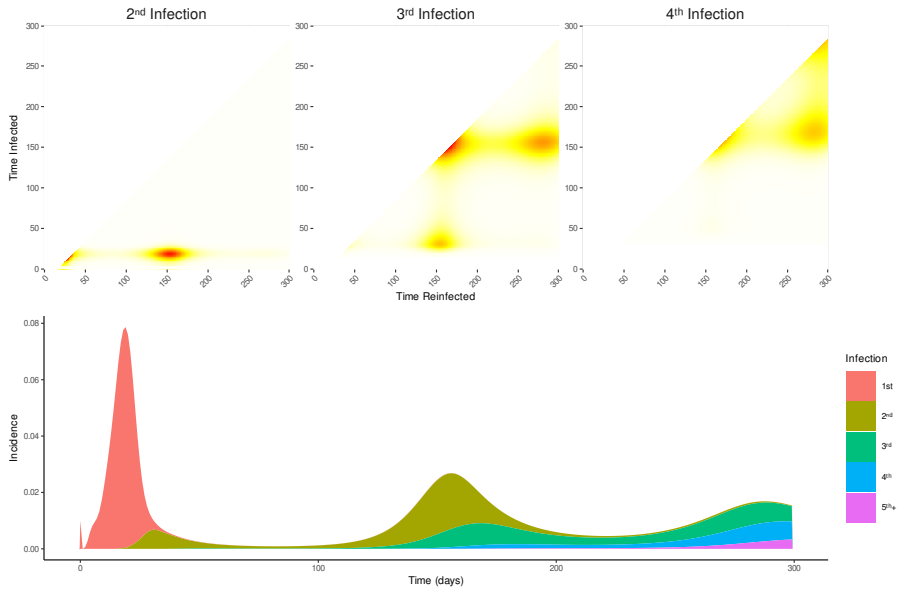

Figure 5: In the top row are transition matrices for the 2nd, 3rd, and 4th infections, showing the probability of last being infected at a time of the vertical axis and then reinfected at a time of the horizontal axis. Darker areas indicate a higher probability and lighter areas a lower probability. The bottom figure is the daily incidence through time, decomposed into which infection an individual is experiencing. Here $K_V = 3 \times 10^6$ and $K_A = 2 \times 10^3$

8 How level of immunity affects epidemiological dynamics

The level of protection conveyed by the immune response induced by exposure is controlled by K_A. Varying K_A is equivalent to rescaling the odds that a correlate/surrogate implies protection. Figure 6 shows the incidence and reinfection dynamics under assumptions of weak protection (high K_A) and strong protection (low K_A).

When weak protection is conveyed an endemic state is quickly reached and reinfection is frequent and rapid. When strong protection is conveyed, defined waves emerge. Initially waves are dominated by the reinfection of those infected in the previous wave, but as the epidemic progress the waves become more mixed. Comparing the dynamics in figures 5 and 6 we can see how decreasing K_A results in more distant waves with initially delineated reinfections.

9 Demonstrating fitting the IIC model to case data

To extract correlates of infectivity and immunity from population-level data with the IIC it must be possible to recover the true values of K_V and K_A when fitting to population-level data. Given a probability of testing positive as a function of viral load,

$$P_P(h) = G(V(h); K_P) \tag{14}$$

with a known K_P (37), and functions of viral load (equation (5)) and immune factor levels (equation (6)), we can estimate K_V and K_A from daily and weekly reported testing data. The proportion of the population testing positive is modelled as

$$T_p(t) = \psi I_0 \theta^S_{0,t} P_P(t) + \psi\xi \int_0^t S(\tau) I_n(\tau) \theta^S_{\tau,t} P_P(t-\tau)\, d\tau, \tag{15}$$

where ψ is the per-person rate of testing.

Using the parameter values in table 2 and $K_V = 3 \times 10^6$, $K_A = 2 \times 10^3$, $\psi = \frac{1}{7}$, and $\xi = 3$ we can simulate an epidemic and model testing data through an over-dispersed, negative-binomial process,

$$p(t) = T_p(t), \tag{16}$$

$$r(t) = \frac{T_p(t) \cdot \text{population} \cdot p(t)}{1 - p(t)}, \tag{17}$$

$$Y(t) \sim NB(r(t), p(t)) \tag{18}$$

$$\tag{19}$$

where $Y_D(t)$ is the tests reported on day t. This formulation ensures that the mean of the distribution is the expected number of positive tests in the population, $T_p(t) \cdot \text{population}$.

9.1 Likelihood and Prior assumptions

Rescaling K_V and K_A to $K'_V = \frac{K_V}{3\times10^6}$ and $K'_A = \frac{K_A}{2\times10^3}$, so that the true value is 1, allows the same prior to be used for both parameters ($A(t)$ and $V(t)$ are rescaled by the same amount). Table 3 contains the 2.5% and 97.5% quantiles of the four different lognormal priors used for K'_V and K'_A. These priors represent potential uncertainties about the initial reproduction number (see appendix C). Initial incidence is also fit with a uniform prior between 0 and 0.01. The mean of a negative binomial process is the same as a Poisson distribution, so, denoting the predicted number positive tests on day t as $X(t; K'_V, K'_A, I_0)$, we assume

$$Y(t) \sim Poisson(X(t; K'_V, K'_A, I_0)). \tag{20}$$

	Prior 1	Prior 2	Prior 3	Prior 4
R_0	[3,5]	[2,6]	[4,7]	[1,5]
K'_V & K'_A	[0.86, 1.6]	[0.68, 2.5]	[0.54, 1.1]	[0.86, 5.3]

Table 3: 2.5% and 97.5% quantiles of the lognormal priors for K'_V and K'_A (rescaled K_V and K_A) based on the assumed initial reproduction number, R_0.

9.2 Fits to daily and weekly reported test data

Figure 7 shows the posterior distributions of K_V, K_A, and I_0 for the four prior assumptions and the resulting fits to the simulated data. We see that the 95% CrI bound the generating process, suggesting the true values of K_V and K_A are recoverable and the model is identifiable.

10 Discussion and conclusion

We develop a flexible and novel mathematical framework that predicts population-level epidemiological dynamics from within-in host virological and immunological data. The framework leverages the full richness of PCR Cq values (38) and assay results, rather than reducing both to binary decisions on infection and sero-positivity, and can incorporate data from many different immunological factors, such as serological IgG, mucosal IgA, and T-cells, separately or in combination. When assuming that infectivity and immunity evolve continuously, and that these are correlated with viral load and immune factor levels, this framework is more accurate than large compartmental models. In addition, this framework can recover the probability that a person has been reinfected, how many infections they are likely to have had, and when each infection is likely to have occurred. These probabilities are estimated from the interaction between within-host immunological processes and the population-level force of infection, inferred from the accumulation of individual viral load. These estimates of protective protective and infectious profiles can be validated by regularly testing individuals for current infection or regular collection of serological data to infer past infection (28). Consequently, this framework allows for the estimation and validation of profiles of protection in individual's with varying immune histories, furthering our understanding population immunity and its consequences for disease dynamics.

Although the IIC model offers greater insight into the effects of immunity and infectivity on the epidemic than equivalent compartmental models, its current form is simple and does not incorporate population heterogeneities, multiple cross-reactive strains, immune responses that vary with the number of exposures, or vaccination. However, the framework can be extended for these purposes.

Implementing extensions that require memory or interaction between the host's current state and future within-host kinetics is more difficult. The current formulation of the IIC model is Markovian. It assumes an individual's viral load

and immune-factor level are reset upon reinfection and therefore levels do not accumulate with each infection. Similarly, it assumes the state of the immune system during infection does not affect viral kinetics. To directly account for the dependency between with-host state at infection and subsequent within-host kinetics, the state space of the model would need to be expanded to consider all possible infection histories up until the time of the current infection, which will become intractable, especially with small time steps.

The viral load level at infection will have negligible impact on subsequent viral load trajectories and disease dynamics if it is assumed that reinfection cannot occur while a current infection is active (while viral load is elevated above the initial viral load). Under this assumption, initial viral load is essentially equal at any time of infection.

As for immune factors, antibody and memory B cell levels at infection have been found to affect antibody and memory B cell levels at the end of the infection (39; 40; 3), with different assumptions about the interaction between past and present infection resulting in substantially different predictions of epidemic trajectory (41). Similarly, we find that changes in the profile of protection have substantially impact on epidemiological dynamics. Hence, the effect of initial immune function level on epidemiological dynamics will need to be investigated before drawing conclusion from the model. How the magnitude of the effect will depend on many factors, such as if the immune function already predicts very strong or very weak protection (changes in the extremes may be negligible due to saturation in the function that transform from immune factor level to probability of protection), if the initial level has much impact of the immune function dynamics, and what function is used to transform from absolute level to probability of protection.

Longitudinal measurements of antibodies and T cells elicited from COVID-19 infection appear to saturate and repeat dynamics after each similar exposure (42; 43; 44), suggesting that a distinction between primary and subsequent infections is adequate. However, the neutralising potential of these antibodies may vary with immune history and further vaccination (44) and the observed saturation could be due to the limits of the assays being reached.

It remains to be seen whether the parameters of the IIC model and its predictions of infection times are accurate when fit to real world case data. For this purpose, it will be necessary to expand the existing model to account for population heterogeneities and include vaccination. This expansion and validation is possible because of the collection of serological data during the COVID-19 pandemic (45).

References

[1] Murphy K, Weaver C. Janeway's Immunobiology. W.W. Norton & Company; 2016.

[2] Le A, King AA, Magpantay FMG, Mesbahi A, Rohani P. The impact of

infection-derived immunity on disease dynamics. Journal of Mathematical Biology. 2021 Nov;83(6–7).

[3] Heffernan JM, Keeling MJ. Implications of vaccination and waning immunity. Proceedings of the Royal Society B: Biological Sciences. 2009 Mar;276(1664):2071-80.

[4] Barnard RC, Davies NG, Munday JD, Lowe R, Knight GM, Leclerc QJ, et al. Modelling the medium-term dynamics of SARS-CoV-2 transmission in England in the Omicron era. Nature Communications. 2022 Aug;13(1).

[5] Hadley E, Yoo YJ, Patel S, Zhou A, Laraway B, Wong R, et al. Insights from an N3C RECOVER EHR-based cohort study characterizing SARS-CoV-2 reinfections and Long COVID. Communications Medicine. 2024 Jul;4(1).

[6] Yoshida N, Fujino M, Miyata A, Nagai T, Kamada M, Sakiyama H, et al. Mumps virus reinfection is not a rare event confirmed by reverse transcription loop-mediated isothermal amplification. Journal of Medical Virology. 2008 Jan;80(3):517-23.

[7] Markwalter CF, Petersen JEV, Zeno EE, Sumner KM, Freedman E, Mangeni JN, et al. Symptomatic malaria enhances protection from reinfection with homologousPlasmodium falciparumparasites. 2023 Jan.

[8] Choi KM. Reemergence of mumps. Korean Journal of Pediatrics. 2010;53(5):623.

[9] Lawpoolsri S, Sattabongkot J, Sirichaisinthop J, Cui L, Kiattibutr K, Rachaphaew N, et al. Epidemiological profiles of recurrent malaria episodes in an endemic area along the Thailand-Myanmar border: a prospective cohort study. Malaria Journal. 2019 Apr;18(1).

[10] Plotkin S. Vaccines: Correlates of Vaccine-Induced Immunity. Clinical Infectious Diseases. 2008 Aug;47(3):401-9.

[11] Plotkin SA. Correlates of Protection Induced by Vaccination. Clinical and Vaccine Immunology. 2010 Jul;17(7):1055-65.

[12] He X, Chandrashekar A, Zahn R, Wegmann F, Yu J, Mercado NB, et al. Low-dose Ad26.COV2.S protection against SARS-CoV-2 challenge in rhesus macaques. Cell. 2021 Jun;184(13):3467-73.e11.

[13] Yu J, Tostanoski LH, Peter L, Mercado NB, McMahan K, Mahrokhian SH, et al. DNA vaccine protection against SARS-CoV-2 in rhesus macaques. Science. 2020 Aug;369(6505):806-11.

[14] Earle KA, Ambrosino DM, Fiore-Gartland A, Goldblatt D, Gilbert PB, Siber GR, et al. Evidence for antibody as a protective correlate for COVID-19 vaccines. Vaccine. 2021 Jul;39(32):4423-8.

[15] Khoury DS, Cromer D, Reynaldi A, Schlub TE, Wheatley AK, Juno JA, et al. Neutralizing antibody levels are highly predictive of immune protection from symptomatic SARS-CoV-2 infection. Nature Medicine. 2021 May;27(7):1205-11.

[16] Goldblatt D, Alter G, Crotty S, Plotkin SA. Correlates of protection against SARS-CoV-2 infection and COVID-19 disease. Immunological Reviews. 2022 Jun;310(1):6-26.

[17] Wei J, Pouwels KB, Stoesser N, Matthews PC, Diamond I, Studley R, et al. Antibody responses and correlates of protection in the general population after two doses of the ChAdOx1 or BNT162b2 vaccines. Nature Medicine. 2022 Feb;28(5):1072-82.

[18] Agency UHS. SARS-CoV-2 variants of concern and variants under investigation in England; 2021.

[19] Agency UHS. Weekly national Influenza and COVID-19 surveillance report Week 40 report (up to week 39 data) 7 October 2021; 2021.

[20] Kermack WO, McKendrick AG. A contribution to the mathematical theory of epidemics. Proceedings of the Royal Society of London Series A, Containing Papers of a Mathematical and Physical Character. 1927 Aug;115(772):700-21.

[21] Wearing HJ, Rohani P, Keeling MJ. Correction: Appropriate Models for the Management of Infectious Diseases. PLoS Medicine. 2005 Aug;2(8):e320.

[22] Lloyd AL. Destabilization of epidemic models with the inclusion of realistic distributions of infectious periods. Proceedings of the Royal Society of London Series B: Biological Sciences. 2001 May;268(1470):985-93.

[23] Blythe SP, Anderson RM. Distributed Incubation and Infectious Periods in Models of the Transmission Dynamics of the Human Immunodeficiency Virus (HIV). Mathematical Medicine and Biology. 1988;5(1):1-19.

[24] Gilchrist MA, Sasaki A. Modeling Host–Parasite Coevolution: A Nested Approach Based on Mechanistic Models. Journal of Theoretical Biology. 2002 Oct;218(3):289-308.

[25] White LJ, Medley GF. Microparasite population dynamics and continuous immunity. Proceedings of the Royal Society of London Series B: Biological Sciences. 1998 Oct;265(1409):1977-83.

[26] Ghosh S, Volpert V, Banerjee M. An Epidemic Model with Time-Distributed Recovery and Death Rates. Bulletin of Mathematical Biology. 2022 Jun;84(8).

[27] Bhattacharya S, Adler FR. A Time Since Recovery Model with Varying Rates of Loss of Immunity. Bulletin of Mathematical Biology. 2012 Oct;74(12):2810-9.

[28] Hay JA, Minter A, Ainslie KEC, Lessler J, Yang B, Cummings DAT, et al. An open source tool to infer epidemiological and immunological dynamics from serological data: serosolver. PLOS Computational Biology. 2020 May;16(5):e1007840.

[29] McMahon A, Robb NC. Reinfection with SARS-CoV-2: Discrete SIR (Susceptible, Infected, Recovered) Modeling Using Empirical Infection Data. JMIR Public Health and Surveillance. 2020 Nov;6(4):e21168.

[30] Viguerie A, Carletti M, Silvestri G, Veneziani A. Mathematical Modeling of Periodic Outbreaks with Waning Immunity: A Possible Long-Term Description of COVID-19. Mathematics. 2023 Dec;11(24):4918.

[31] Rodriguez-Maroto G, Atienza-Diez I, Ares S, Manrubia S. Vaccination strategies in structured populations under partial immunity and reinfection. Journal of Physics A: Mathematical and Theoretical. 2023 Apr;56(20):204003.

[32] Stocks D, Thomas A, Finn A, Danon L, Brooks-Pollock E. Mechanistic models of humoral kinetics following COVID-19 vaccination. Journal of The Royal Society Interface. 2025 Jan;22(222).

[33] Killingley B, Mann AJ, Kalinova M, Boyers A, Goonawardane N, Zhou J, et al. Safety, tolerability and viral kinetics during SARS-CoV-2 human challenge in young adults. Nature Medicine. 2022 Mar;28(5):1031-41.

[34] Wearing HJ, Rohani P, Keeling MJ. Appropriate Models for the Management of Infectious Diseases. PLoS Medicine. 2005 Jul;2(7):e174.

[35] Hurtado PJ, Kirosingh AS. Generalizations of the 'Linear Chain Trick': incorporating more flexible dwell time distributions into mean field ODE models. Journal of Mathematical Biology. 2019 Aug;79(5):1831-83.

[36] Krylova O, Earn DJD. Effects of the infectious period distribution on predicted transitions in childhood disease dynamics. Journal of The Royal Society Interface. 2013 Jul;10(84):20130098.

[37] Eyre DW, Futschik M, Tunkel S, Wei J, Cole-Hamilton J, Saquib R, et al. Performance of antigen lateral flow devices in the UK during the alpha, delta, and omicron waves of the SARS-CoV-2 pandemic: a diagnostic and observational study. The Lancet Infectious Diseases. 2023 Aug;23(8):922-32.

[38] Hay JA, Kennedy-Shaffer L, Kanjilal S, Lennon NJ, Gabriel SB, Lipsitch M, et al. Estimating epidemiologic dynamics from cross-sectional viral load distributions. Science. 2021 Jul;373(6552).

[39] Diekmann O, de Graaf WF, Kretzschmar MEE, Teunis PFM. Waning and boosting: on the dynamics of immune status. Journal of Mathematical Biology. 2018 May;77(6–7):2023-48.

[40] de Graaf WF, Kretzschmar MEE, Teunis PFM, Diekmann O. A two-phase within-host model for immune response and its application to serological profiles of pertussis. Epidemics. 2014 Dec;9:1-7.

[41] Barbarossa MV, Polner M, Röst G. Temporal Evolution of Immunity Distributions in a Population with Waning and Boosting. Complexity. 2018 Jan;2018(1).

[42] Regev-Yochay G, Gonen T, Gilboa M, Mandelboim M, Indenbaum V, Amit S, et al. Efficacy of a Fourth Dose of Covid-19 mRNA Vaccine against Omicron. New England Journal of Medicine. 2022 Apr;386(14):1377-80.

[43] Rubio R, Macià D, Barrios D, Vidal M, Jiménez A, Molinos-Albert LM, et al. High-resolution kinetics and cellular determinants of SARS-CoV-2 antibody response over two years after COVID-19 vaccination. Microbes and Infection. 2025 Feb;27(2):105423.

[44] Belik M, Liedes O, Vara S, Haveri A, Pöysti S, Kolehmainen P, et al. Persistent T cell-mediated immune responses against Omicron variants after the third COVID-19 mRNA vaccine dose. Frontiers in Immunology. 2023 Jan;14.

[45] Atti A, Insalata F, Carr EJ, Otter AD, Castillo-Olivares J, Wu M, et al. Antibody correlates of protection from SARS-CoV-2 reinfection prior to vaccination: A nested case-control within the SIREN study. Journal of Infection. 2022 Nov;85(5):545-56.

[46] Hernandez-Vargas EA, Velasco-Hernandez JX. In-host Mathematical Modelling of COVID-19 in Humans. Annual Reviews in Control. 2020;50:448-56.

A The trapezoidal approximation of the IIC model

The trapezium rule approximates the integral between 0 and t by summing the areas of trapezoids of width Δt. This approximation allows $I(t)$ and $S(t)$ to be solved iteratively (in steps of Δt) as they can be written entirely in terms of previous (already calculated) values.

A.1 Solving $\theta_{\tau,t}$

By splitting $\theta_t^{S_0}$ and $\theta_{\tau,t}^S$ by into all previous time steps $[0,\, t-\Delta t]$ and the current time-step $[t-\Delta t,\, t]$ we can represent $\theta_t^{S_0}$ and $\theta_{\tau,t}^S$ as the product their previous values, $\theta_{\tau,t-\Delta t}^S$ and $\theta_{t-\Delta t}^{S_0}$, and infectious pressure in the current time-step.

$$\begin{aligned}\theta_{\tau,t}^S &= \exp\left(-\xi \int_0^{t-\tau} P_S(s)\, I_n(\tau+s)\, ds\right)\\ &= \exp\left(-\xi \int_0^{t-\Delta t-\tau} P_S(s)\, I_n(\tau+s)\, ds - \xi \int_{t-\Delta t-\tau}^{t-\tau} P_S(s)\, I_n(\tau+s)\, ds\right)\\ &= \theta_{\tau,t-\Delta t} \cdot \exp\left(-\xi \int_{t-\Delta t-\tau}^{t-\tau} P_S(s)\, I_n(\tau+s)\, ds\right).\end{aligned} \tag{21}$$

By the trapezoidal rule,

$$\int_{t-\Delta t-\tau}^{t-\tau} P_{S,s}\, I_n(\tau+s)\, ds \approx \frac{\Delta t}{2}\big(P_S(t-\Delta_t-\tau)I_n(t-\Delta_t)+P_S(t-\tau)I_n(t)\big). \tag{22}$$

Hence,

$$\theta_{\tau,t} \approx \theta_{\tau,t-\Delta_t} \cdot \exp\Big(-\frac{\xi\Delta_t}{2}\big(P_S(t-\Delta_t-\tau)I_n(t-\Delta_t)+P_S(t-\tau)I_n(t)\big)\Big). \tag{23}$$

Once $I_n(t)$ is known equation (23) can be used to update $\theta_{\tau,t}$ for the next iteration (when it will become $\theta_{\tau,t-\Delta_t}$). However, when calculating $I_n(t)$ in the current iteration we must use the approximation $e^{-x} \approx (1-x)$ (valid for small Δ_t), so that $I_n(t)$ can be isolated. Hence,

$$\theta_{\tau,t} \approx \theta_{\tau,t-\Delta_t} F_{\tau,t-\Delta_t}(1 - AP_S(t-\tau)I_n(t)), \tag{24}$$

where $F_{\tau,t-\Delta_t} = \exp\big(-AP_S(t-\Delta_t-\tau)I_n(t-\Delta_t)\big)$ and $A = \frac{\xi\Delta_t}{2}$.

A.2 Solving $I_n(t)$ and $P(t)$ for $t = 0$

$$I_n(0) = I_0 P_I(0), \tag{25a}$$

$$S(0) = (S_0 + I_0)P_S(0). \tag{25b}$$

A.3 Solving $I_n(t)$ and $P(t)$ for $t > \Delta_t$

By the trapezoidal rule, for $t > \Delta_t$,

$$\begin{aligned} I_n(t) \approx & I_0 P_I(t)\theta^S_{0,t} + A\Big(S(0)I_n(0)\theta^S_{0,t}P_I(t) + S(t)I_n(t)\theta^S_{t,t}P_I(0) \\ & + 2\sum_{i=\Delta_t}^{t-\Delta_t} \theta^S_{i,t}S(i)I_n(i)P_I(t-i)\Big), \end{aligned} \tag{26}$$

$$\begin{aligned} S(t) \approx & S_0\theta^{S_0}_t + I_0\theta^S_{0,t}P_P(t) + A\Big(S(0)I_n(0)\theta^S_{0,t}P_P(t) + S(t)I_n(t)\theta^S_{t,t}P_S(0) \\ & + 2\sum_{i=\Delta_t}^{t-\Delta t} \theta^S_{i,t}S(i)I_n(i)P_S(t-i)\Big). \end{aligned} \tag{27}$$

Substituting in equation (24) and setting $\theta_{t,t} = 1$ we can define

$$\begin{aligned} B_I =& I_0\, \theta^S_{0,t-\Delta t}\, F^S_{0,t-\Delta t} P_I(t), \\ C_I =& S(0)I_n(0)\, \theta^S_{0,t-\Delta t}\, F^S_{0,t-\Delta t}\, P_I(t), \\ D_I =& 2\sum_{i=\Delta t}^{t-\Delta t} S(i)I_n(i)\, \theta^S_{i,t-\Delta t}\, F^S_{i,t-\Delta t}\, P_I(t-i), \\ E_I =& 2\sum_{i=\Delta t}^{t-\Delta t} S(i)I_n(i)\, \theta^S_{i,t-\Delta t}\, F^S_{i,t-\Delta t}\, P_S(t-i)P_I(t-i), \\ B_S =& S_0\, \theta^{S_0}_{t-\Delta t}\, F^{S_0}_{t-\Delta t}, \\ \bar{B}_S =& I_0\theta^S_{0,t-\Delta t}\, F^S_{0,t-\Delta t}\, P_S(t) \\ C_S =& S(0)I_n(0)\, \theta^S_{0,t-\Delta t}\, F^S_{0,t-\Delta t}\, P_S(t), \\ D_S =& 2\sum_{i=\Delta t}^{t-\Delta t} S(i)I_n(i)\, \theta^S_{i,t-\Delta t}\, F^S_{i,t-\Delta t}\, P_S(t-i), \\ E_S =& 2\sum_{i=\Delta t}^{t-\Delta t} S(i)I_n(i)\, \theta^S_{i,t-\Delta t}\, F^S_{i,t-\Delta t}\, P_S(t-i)^2, \end{aligned}$$

and rewrite equations (26) and (27),

$$\begin{aligned} S(t) \approx & B_S + \bar{B}_S + AC_P + AD_P \\ & - A(B_S + \bar{B}_S P_S(t) + AC_S P_S(t) + AE_P)I_n(t) \\ & + AS(t)I_n(t)P_S(0) \end{aligned} \tag{28}$$

$$\begin{aligned} I_n(t) \approx & B_I + AC_I + AD_I \\ & - A(B_I P_S(t) + AC_I P_S(t) + AE_I)I_n(t) \\ & + AS(t)I_n(t)P_I(0). \end{aligned} \tag{29}$$

To make equations (28) and (29) more readable we define,

$$\begin{aligned}
B_{S,2} &= B_S + \bar{B}_S + AC_P + AD_P, \\
C_{S,2} &= A(B_S + \bar{B}_S P_S(t) + AC_S P_S(t) + E_P), \\
B_{I,2} &= B_I + AC_I + AD_I, \\
C_{I,2} &= A(B_I P_S(t) + AC_I P_S(t) + E_I).
\end{aligned}$$

We rearrange equation (28) to make $S(t)$ the subject,

$$S(t) \approx \frac{B_{S,2} - C_{S,2} I_n(t)}{1 - AI_n(t) P_S(0)}. \tag{30}$$

and substitute into equation (29), which can then be rearranged into the quadratic,

$$\begin{aligned}
0 \approx B_{I,2} &+ (AB_{S,2} P_I(0) - C_{I,2} - AB_{I,2} P_S(0) - 1) I_n(t) \\
&+ A(C_{I,2} P_S(0) + AP_S(0) - AC_{S,2} P_I(0)) I_n^2(t).
\end{aligned} \tag{31}$$

The negative solution of this quadratic gives positive values of $I_n(t)$. This solution can be substituted back into equation (30) to give $S(t)$. If it is assumed that $P_S(0) = P_I(0) = 0$ (an individual cannot be immediately reinfected and is not immediately infectious) equations (31) reduce to a first-order polynomial.

A.4 Solving $I_n(t)$ and $P(t)$ for $t = \Delta_t$

When $t = \Delta_t$ there is a single trapezoid, so setting $D_I, D_P, E_I, E_P = 0$ equations (30) and (31) will provide the solutions to $S(\Delta t)$ and $I_n(\Delta t)$ respectively.

A.5 Including an Auxiliary Testing Variable

For fitting to testing data (number of positive tests received across the population) we can calculate the proportion of the population testing positive, $T_p(t)$, by assuming there is an average rate of testing per unit time, ψ, and a function $P_P(h) : R \to [0, 1]$ that defines the probability of testing positive h units time after an infection.

$$\begin{aligned}
T_p(t) &= \psi I_0 \theta^S_{0,t} P_P(t) + \psi \xi \int_0^t S(\tau) I_n(\tau) \theta^S_{\tau,t} P_P(t - \tau)\, d\tau, \\
&\approx \psi I_0 \theta^S_{0,t} P_P(t) + \psi A \Bigg(S(0) I_n(0) \theta^S_{0,t} P_P(t) + S(t) I_n(t) \theta^S_{t,t} P_P(0) \\
&\qquad + 2 \sum_{i=\Delta t}^{t-\Delta t} S(i) I_n(i) \theta^S_{i,t} P_P(t - i) \Bigg).
\end{aligned} \tag{32}$$

Substituting in equation (24) and setting $\theta_{t,t} = 1$ we get,

$$\begin{aligned}
T_P(t) \approx\ & \psi I_0[\theta^S_{0,t-\Delta t} F_{0,t-\Delta t}(1 - AP_S(t)I_n(t))]P_P(0) \\
& + \psi A \Bigg(S(0)I_n(0)[\theta^S_{0,t-\Delta t} F^S_{0,t-\Delta t}(1 - AP_S(t)I_n(t))]P_P(t) \\
& \quad + S(t)I_n(t)P_P(0) \\
& \quad + 2\sum_{i=\Delta t}^{t-\Delta t} S(i)I_n(i)[\theta^S_{i,t-\Delta t} F^S_{i,t-\Delta t}(1 - AP_S(t-i)I_n(t))]P_P(t-i) \Bigg).
\end{aligned} \tag{33}$$

Since $T_p(t)$ does not affect the dynamics of the epidemic, it is not necessary to rewrite equation 33. However, for consistency and readability, we define

$$\begin{aligned}
B_P &= I_0 \theta^S_{t-\Delta t} F^S_{0,t-\Delta t} P_P(t), \\
C_P &= S(0)I_n(0)\theta^S_{0,t-\Delta t} F^S_{0,t-\Delta t} P_P(t), \\
D_P &= 2\sum S(i)I_n(i)\theta^S_{i,t-\Delta t} F^S_{i,t-\Delta t} P_P(t-i), \\
E_P &= 2\sum S(i)I_n(i)\theta^S_{i,t-\Delta t} F^S_{i,t-\Delta t} P_P(t-i)P_S(t-i), \\
B_{P,2} &= \psi(B_P + AC_P + AD_P), \\
C_{P,2} &= \psi A(B_P P_S(t) + AC_P P_S(t) + AE_P),
\end{aligned}$$

giving

$$T_P(t) = B_{P,2} - C_{P,2} I_n(t) + \psi A S(t) I_n(t) P_P(0) \tag{34}$$

B Modeling viral load

An established model of viral load is the target cell-limited (TCL) model consisting of target cells, T, infected cells, I, and virus, V. Their dynamics are described as,

$$\dot{T}(t) = -\beta TV, \tag{35a}$$

$$\dot{I}(t) = \beta TV - \gamma I, \tag{35b}$$

$$\dot{V}(t) = \rho I - \delta V, \tag{35c}$$

where β is the rate virus infects target cells, γ is the rate infected cells die, ρ is the rate infected cells produce virus, and δ is the rate virus dies. Neither replication nor death of target cells is considered as the model is over a short time frame, with the dynamics dominated by infection. The immune response is also not explicitly considered but its presence will affect estimations of β and γ when the model is fit to viral load data.

As we aim to describe the temporal dynamics of viral load rather than explain the driving mechanisms, the function

$$V(h) = (h + d)^{\alpha - 1} e^{-\kappa(h+d)}, \tag{36}$$

TCL Model Prior Assumptions					
β	γ	ρ	δ	T_0	V_0
$[7.5 \times 10^{-8}, 21.3 \times 10^{-5}]$	[0.71, 1.91]	[0.2, 0.6]	[0.5, 4]	$[2 \times 10^7, 3 \times 10^9]$	$[10^4, 10^6]$

Gamma Model Prior Assumptions		
d	α	κ
[1, 5]	[1, 10]	$[10^{-4}, 2]$

Table 4: The 2.5% and 97.5% quantiles of the model parameter's and initial condition's prior distributions. The assumptions for the TCL model are based on estimates in (46), except for V_0, where assumptions are based on prior predictive checks. The assumptions for the gamma model are based on prior predictive checks.

is proposed as a model, where d shifts the function to allow for non-zero values at $h = 0$ and α and κ are shape and rate parameters. This model will be referred to as the gamma model.

B.1 Model fitting

We use viral load data from a SARS-CoV-2 human challenge study collected via throat swab from 18 18 – 29 year-olds, who were seronegative and had not been vaccinated (33).

We fit the models to viral data using Markov chain Monte Carlo methods. Table 4 contains prior distribution assumptions, based on previous modeling in (46) and prior predictive checks. We assume the viral load data is log-normally distributed, with a mean described by the models. We used a multivariate distribution to preserve individual information while estimating the population mean.

B.2 Comparing the fits

Figure 8 shows the model fits to the data. Comparing the models by the Bayesian information criterion (2586 for the gamma model and 2651 for the TCL model) we find the gamma model better describes the data better than the TCL model.

C The Reproduction Number

The reproduction number quantifies the average number of people an average individual will infect throughout a single infection. The basic reproduction number, R_0, is the average number of people infected in an entirely susceptible population, and the instantaneous reproduction number, R_t, is the average number of people an individual infected at time t will subsequently infect. For

the SIR and SIRS models with full immunity after infection,

$$R_0 = \frac{\beta}{\phi} \;=\; \frac{\xi\eta}{\phi} \;=\; \xi \int_0^{\frac{1}{\phi}} P_I(h)\, dh \tag{37}$$

$$R_t = \frac{\beta}{\phi} S(t) \;=\; \xi S(t) \int_0^{\frac{1}{\phi}} P_I(h)\, dh. \tag{38}$$

When immunity after infection is partial R_0 remains the same but

$$R_t = \frac{\beta}{\phi}(S(t) + \delta R(t)) \tag{39}$$

When there are multiple infectious states

$$R_0 = \frac{\xi}{n\phi} \sum_{i=i}^{n} \eta_i, \tag{40}$$

$$R_t = \frac{\xi}{n\phi} \sum_{i=1}^{n} \eta_i \Big(S(t) + \sum_{j=1}^{m} \delta_j R_j(t) \Big). \tag{41}$$

Comparatively, for the IIC model,

$$R_0 = \xi \int_0^{\infty} P_I(h)\, dh \tag{42}$$

$$R_t^b = \xi S(t) \int_0^{\infty} P_I(h)\, dh, \tag{43}$$

$$R_t^f = \xi \int_t^{\infty} S(\tau)\, P_I(t-\tau) \theta_{\tau,t}\, d\tau. \tag{44}$$

where R_t^b is the backward reproduction number, which is equivalent to the instantaneous reproduction number, R_t, calculated for compartmental models, and R_t^f is the forward reproduction number. R_t^b assumes immunity in the population remains constant and therefore measures the number of people an individual infected at time t could infect within the immune landscape at t; the current infectious potential of a newly infected person. Whereas, R_t^f accounts for evolving immunity and quantifies the actual number of people an individual infected at t will subsequently infect. Hence, R_t^b lags R_t^f and $R_t^b = 1$ at the peak of the epidemic, while $R_t^f = 1$ before the peak and predicts the generation of infected that will cause the peak. However, R_t^f is only accurate as $\theta_{\tau,t}^S \to 0$ (generation t has been reinfected) or $P_I(h) \to 0$ (generation t is no longer infectious).

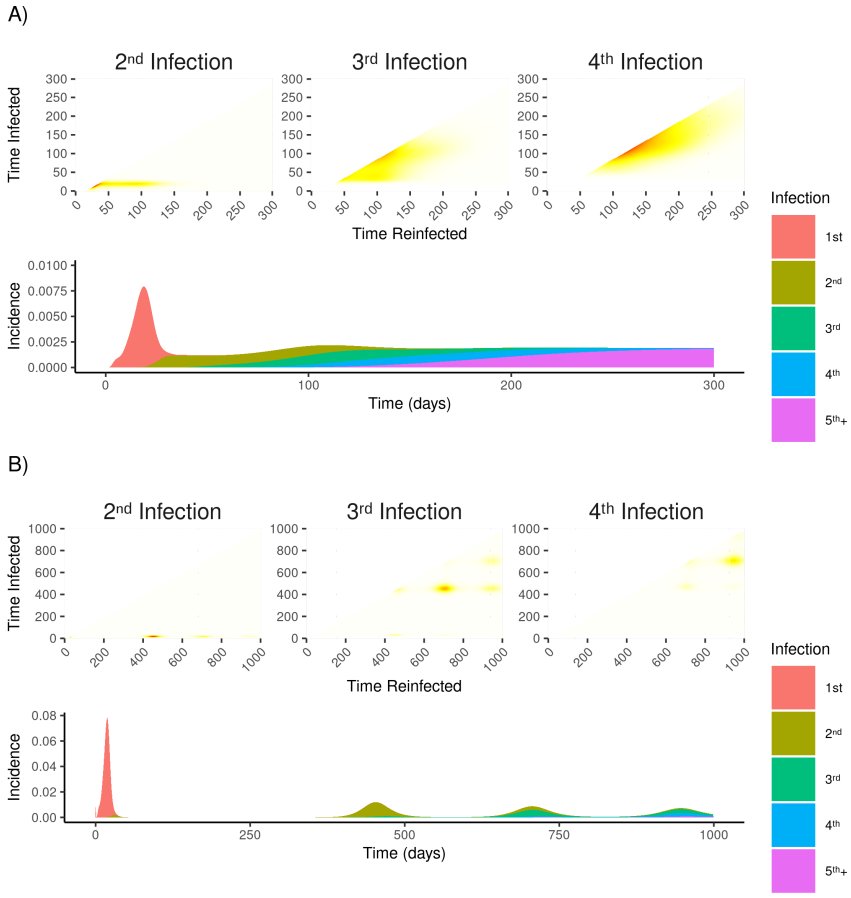

Figure 6: In the top row are transition matrices for the 2nd, 3rd, and 4th infections, showing the probability of last being infected at a time of the vertical axis and then reinfected at a time of the horizontal axis. Darker areas indicate a higher probability and lighter areas a lower probability. The bottom figure is the daily incidence through time, decomposed into which infection an individual is experiencing. In A) $K_V = 3 \times 10^6$ and $K_A = 4 \times 10^3$. In B) $K_V = 3 \times 10^6$ and $K_A = 0.5 \times 10^3$

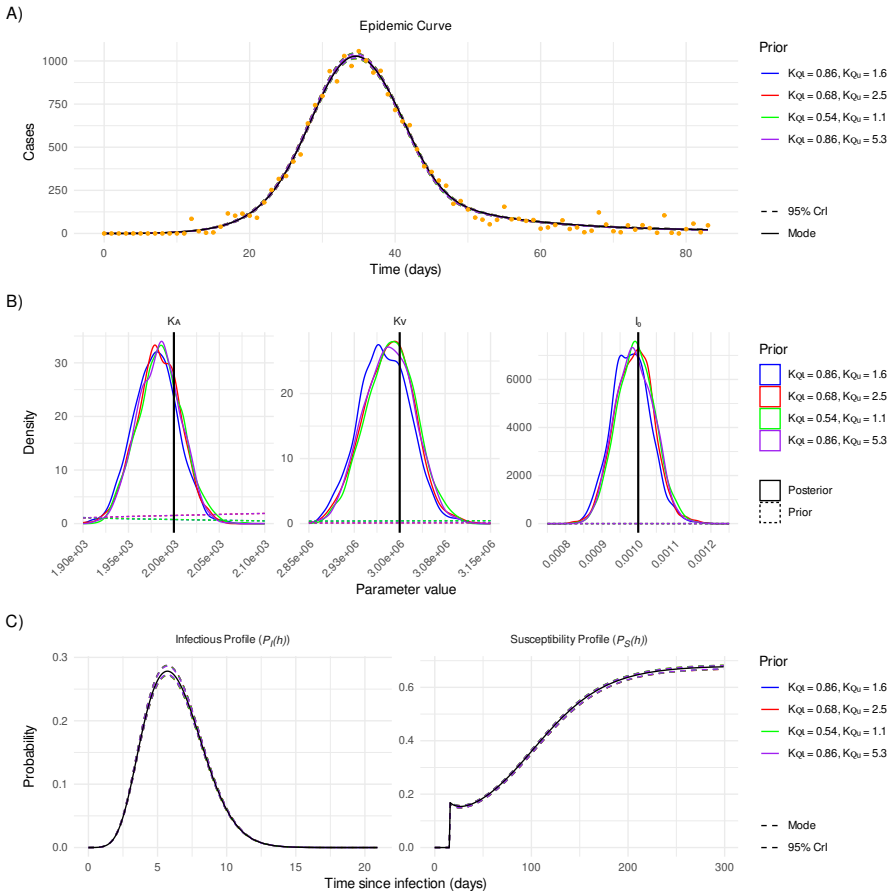

Figure 7: A) The model dynamics fitted to simulated case data with mode and 95% CrI. B) The estimated posterior distributions of initial incidence, I_0, and the scaling parameters for viral load and binding antibody, K_V and K_A respectively. The vertical black lines are the true value of the parameters. C) The predicted infectious and susceptibility profiles.

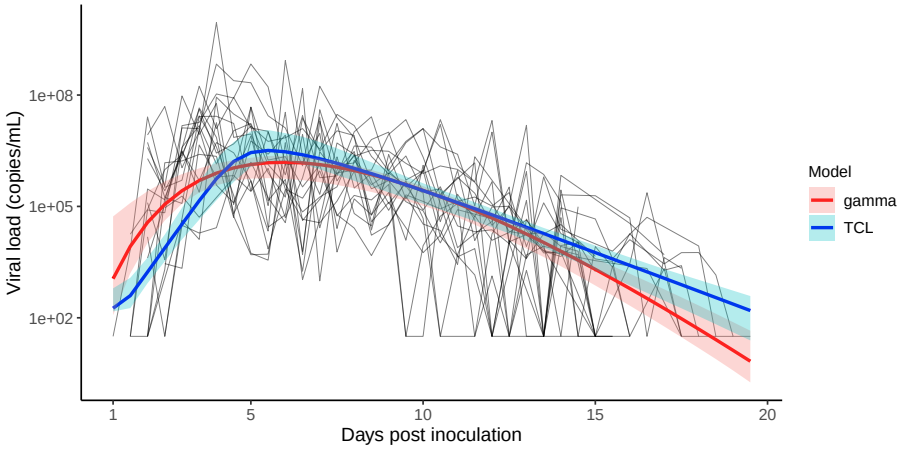

Figure 8: The best fit (solid line) and 95% CrI of the gamma and TCL model fits to viral load data from 18 seronegative, unvaccinated people between 18 and 19 years-old (black lines) (33).